# A Curved-Beam Bistable Mechanism

Jin Qiu, Jeffrey H. Lang, *Fellow, IEEE*, and Alexander H. Slocum, *Member, IEEE*

***Abstract*—This paper presents a monolithic mechanically-bistable mechanism that does not rely on residual stress for its bistability. The typical implementation of this mechanism is two curved centrally-clamped parallel beams, hereafter referred to as "double curved beams". Modal analysis and finite element analysis (FEA) simulation of the curved beam are used to predict, explain, and design its bistable behavior. Microscale double curved beams are fabricated by deep-reactive ion etching (DRIE) and their test results agree well with the analytic predictions. Approaches to tailor the bistable behavior of the curved beams are also presented. [1079]**

***Index Terms*—Beam analysis, bistable structure, compliant structure, deep-reactive ion etching (DRIE), microelectromechanical systems (MEMS), structure optimization.**

## I. Introduction

MECHANICALLY BISTABLE mechanisms are useful in MEMS devices such as relays, valves, clips, threshold switches and memory cells, etc. One advantage of such mechanisms is that they can apply a contact force without the need for continued actuation power. Three main categories of bistable mechanisms have been reported in the MEMS literature: latch-lock mechanisms [1], [2], hinged multisegment mechanisms [3]–[5], and residual-compressive-stress buckled beam or membrane mechanisms [6]–[8]. The latch-lock mechanisms require complex actuation to lock and unlock. Hinges having zero friction, zero clearance, and zero stiffness are hard to realize in general with MEMS fabrication processes, and especially with deep-reactive ion etching (DRIE). Finally, residual stress is hard to realize or control in bulk-fabricated structures. A monolithic bistable mechanism is presented in this paper that uses no latches, no hinges, and no residual stress to achieve its bistability. This mechanism can be effectively fabricated using DRIE [9], and is used in a MEMS relay [10].

Anyone holding a business card between thumb and forefinger to provide an axial force that bows the card can experience the principle of a bistable system. A normal force on the card can cause it to snap through to its second stable position. Constructing such a prestressed bistable system using MEMS technologies, however, can be a difficult task. If one were to make a structure with initial curved shape, without prestress as would be obtained by merely etching a bow-shape, the system may buckle and snap with external force applied but will not stay at the snapped shape when the external force is released due to the occurrence of a twisting buckling mode. This will be proven mathematically in detail below. However, using the principle of reciprocity, the twisting buckling mode in *two* single curved beams can be used to mutually cancel each other yielding a bistable double-beam without prestress. This is achieved by rigidly coupling the two curved beams together at their midpoints.

The clamped double beams structure has been reported before by others, such as in [11] and [12]. Attempts are made to show with a lowest-mode analysis in [11] that a single beam can be made bistable, although it will be shown below that this analysis does not reveal key design requirements. In [12], a comb drive is used to actuate a bar that connects the two beams and also holds optical switch components. The ends of the bar appear to be guided by trenches, and no mention is made of the conditions placed on the beam geometries that are required for bistability. Indeed, the clamped double beams structure is not bistable if the geometries are not carefully selected. Furthermore, it will be shown that a varying cross-section single beam without prestress can be made bistable by thickness modulation; however, the stress state in the modulated beam is several times higher than that in a uniform cross-section beam. In what follows, bistability analysis will be presented in detail, as will a discussion of the fabrication and testing of the bistable structure.

## II. Modeling of Curved Beam

The design of the curved-beam bistable mechanism is inspired from bistable buckled straight-beam mechanisms, where a straight beam is axially compressed to buckle to stable positions at either side. Modeling buckling modes of the latter mechanism is critical to modeling the curved-beam mechanism. The beam equation describing a straight beam subjected to an axial load $p$ is

$$EI\frac{d^4w}{dx^4}+p\frac{d^2w}{dx^2}=0 \tag{1}$$

where $w$ is the lateral beam displacement, $E$ is the Young's modulus of the beam material and $I$ the moment of inertia of the beam. With clamped-clamped conditions, the boundary conditions to (1) are

$$w(0)=w(l)=0,\quad \left(\frac{dw}{dx}\right)_{x=0}=\left(\frac{dw}{dx}\right)_{x=l}=0. \tag{2}$$

Normalize the axial force by

$$N^2=\frac{pl^2}{EI}. \tag{3}$$

Manuscript received June 26, 2003; revised October 31, 2003. This work was supported by ABB corporate research, Baden-Dattwil, Switzerland. Fabrication was performed in the Microsystems Technology Laboratories of MIT. Subject Editor C.-J. Kim.

J. Qiu is with the Tyco Electronics, Menlo Park, CA 94025 USA (e-mail: jqiu@alum.mit.edu).

J. H. Lang is with the Department of Electrical Engineering and Computer Science, Massachusetts Institute of Technology, Cambridge, MA 02139 USA.

A. H. Slocum is with the Department of Mechanical Engineering, Massachusetts Institute of Technology, Cambridge, MA 02139 USA.

Digital Object Identifier 10.1109/JMEMS.2004.825308

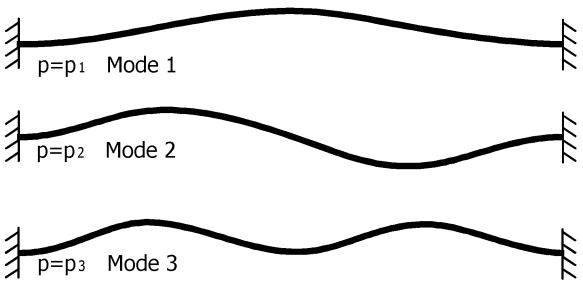


Fig. 1. The first three buckling modes for a clamped-clamped beam.

In order to have nonzero solutions, $N$ must satisfy

$$\sin\left(\frac{N}{2}\right)\left[\tan\left(\frac{N}{2}\right)-\frac{N}{2}\right]=0 \tag{4}$$

which allows two kinds of solution, namely

$$\left.\begin{array}{l} w_j(x)=C\left[1-\cos\left(N_j\frac{x}{l}\right)\right] \\ N_j=(j+1)\pi \end{array}\right\} \quad \mathrm{j}=1,3,5\ldots \tag{5}$$

and

$$\left.\begin{array}{l} w_j(x)=C\left[1-2\frac{x}{l}-\cos\left(N_j\frac{x}{l}\right)+\frac{2\sin\left(N_j\frac{x}{l}\right)}{N_j}\right] \\ N_j=2.86\pi,\ 4.92\pi\ldots \end{array}\right\} \quad j=2,4,6\ldots. \tag{6}$$

The analysis above gives a mathematical foundation for a buckling analysis. The first three modes found from this analysis are shown in Fig. 1. A common bistable mechanism involves a prestressed straight beam buckled into its first mode [6]. Since buckling can take either an up or down direction, this creates two stable positions for the mechanism. The residual stress that gives rise to the axial load is not easy to obtain and control in MEMS devices especially in bulk micro machining. An alternative design that eliminates the need for prestress is to have an as-fabricated stress-free curved beam with an initial first-buckling-mode shape. The analysis below models such a structure to determine the parameter requirements for bistability.

Consider the single beam shown in Fig. 2. It has thickness $t$, depth $b$, span $l$, Young's modulus $E$ and moment of inertia $I$. Let $w(x)$ denote the distance of the beam from the straight line connecting its two boundaries. The as-fabricated shape of the beam is

$$\bar{w}(x)=\frac{h}{2}\left[1-\cos\left(2\pi\frac{x}{l}\right)\right] \tag{7}$$

where $h$ is the initial apex height of the beam. It will be explained later that having such an initial shape is one of several requirements for a curved beam to be bistable. Also as can be seen later in the modeling, the geometry constant $Q$ is critical to the behavior of this mechanism, and it is defined as

$$Q=\frac{h}{t}. \tag{8}$$

As the lateral force $f$ is applied to the center of the beam at $x=l/2$, the center of the beam deflects by

$$d=\bar{w}\left(\frac{l}{2}\right)-w\left(\frac{l}{2}\right). \tag{9}$$

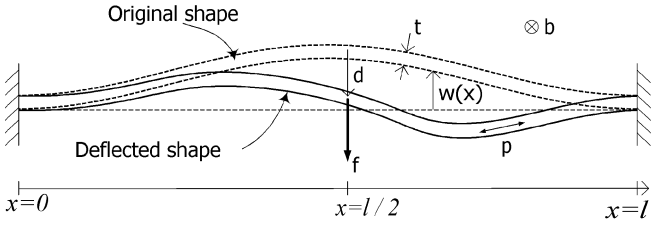


Fig. 2. Geometry and notation for curved beam deflection analysis.

The total length of the beam $s$ changes to

$$s=\int_0^l\sqrt{1+\left(\frac{dw}{dx}\right)^2}dx\approx\int_0^l\left[1+\frac{1}{2}\left(\frac{dw}{dx}\right)^2\right]dx \tag{10}$$

where a small deflection assumption is used. The change of $s$ gives rise to the axial force $p$ by Hooke's law such that

$$p=Ebt\left(1-\frac{s}{(s)_{w=\bar{w}}}\right). \tag{11}$$

During deflection, define $u_b$ as the beam bending energy, $u_s$ as the beam compression energy, and $u_f$ as the actuation energy. The variation of the bending energy inside the beam is

$$\partial(u_b)=\partial\left[\frac{EI}{2}\int_0^l\left(\frac{d^2\bar{w}}{dx^2}-\frac{d^2w}{dx^2}\right)^2dx\right]. \tag{12}$$

The variation of the compression energy inside the beam is

$$\partial(u_s)=-p\partial(s). \tag{13}$$

The variation of the actuation energy is

$$\partial(u_f)=-f\partial(d). \tag{14}$$

A mode superposition method is used in this paper to solve the beam deflection. The buckling modes for the straight clamped-clamped beam given in (5) and (6) form an orthogonal set, so they can be used as the superposition basis for deflection shape of the initially curved beam, which has the same boundary condition with the initially straight beam. While it is possible to solve the problem by using other orthogonal mode shapes having the same boundary condition, using the buckling modes as the superposition basis would best capture the buckling physics of the curved beam during deflection. It could be seen later that the first three buckling modes, as shown in Fig. 1, play significantly roles in determining the deflection of the initially curved beam. To simplify the superposition, first normalize the parameters according to

$$X=\frac{x}{l},\quad W(X)=\frac{w(Xl)}{h}. \tag{15}$$

Then the superposition of the beam shape is

$$W(X)=\sum_{j=1}^{\infty}A_jW_j(X) \tag{16}$$

where

$$\left.\begin{array}{l} W_j(X) = 1 - \cos(N_j X) \\ N_j = (j+1)\pi \end{array}\right\} \quad \mathrm{j} = 1,3,5\ldots \tag{17}$$

and

$$\left.\begin{array}{l} W_j(x) = 1 - 2X - \cos(N_j X) + \frac{2\sin(N_j X)}{N_j} \\ N_j = 2.86\pi,\ 4.92\pi\ldots \end{array}\right\} \quad j = 2,4,6\ldots. \tag{18}$$

The normalized beam shape as fabricated is

$$\bar{W}(X) = \frac{1}{2} W_1(X). \tag{19}$$

Next, normalize the applied force $f$ and parameters in (9)–(14) according to

$$\begin{aligned} F &= \frac{fl^3}{EIh}, \quad \Delta = \frac{d}{h}, \quad S = \frac{sl}{h^2}, \quad N^2 = \frac{pl^2}{EI}, \\ U_b &= \frac{u_b l^3}{EIh^2}, \quad U_s = \frac{u_s l^3}{EIh^2}, \quad U_f = \frac{u_f l^3}{EIh^2}. \end{aligned} \tag{20}$$

With the normalizations in (15) and (20), and the mode superposition in (16)–(19), the relations in (9)–(14) can now be expressed as

$$\Delta = 1 - 2 \sum_{j=1,5,9,13\ldots} A_j \tag{21}$$

$$S = 1 + \sum_{j=1}^{\infty} \frac{A_j^2 N_j^2}{4} \tag{22}$$

$$\frac{N^2}{12Q^2} = (S)_{W=\bar{W}} - S = \frac{N_1^2}{16} - \sum_{j=1}^{\infty} \frac{A_j^2 N_j^2}{4} \tag{23}$$

$$\partial(U_b) = \partial \left[ \frac{\left(\frac{1}{2} - A_1\right)^2 N_1^4}{4} + \sum_{j=2}^{\infty} \frac{A_j^2 N_j^4}{4} \right] \tag{24}$$

$$\partial(U_s) = -N^2 \partial(S) = -N^2 \partial \left( \sum_{j=1}^{\infty} \frac{A_j^2 N_j^2}{4} \right) \tag{25}$$

$$\partial(U_f) = -F \partial(\Delta) = 2F \sum_{j=1,5,9,13\ldots} A_j. \tag{26}$$

Note that all variables can be expressed in terms of the mode amplitudes without any cross-terms. The variation of the total energy within the mechanism $U_t$ is the sum of (24)–(26), and is given by

$$\begin{aligned} \partial(U_t) = &\left( \frac{N_1^4 - N^2 N_1^2}{2} A_1 - \frac{N_1^4}{4} + 2F \right) \partial(A_1) \\ &+ \sum_{j=2,3,4,6,7\ldots} \left( \frac{N_j^4 - N^2 N_j^2}{4} \right) \partial\left(A_j^2\right) \\ &+ \sum_{j=5,9,13\ldots} \left( \frac{N_j^4 - N^2 N_j^2}{2} A_j + 2F \right) \partial(A_j). \end{aligned} \tag{27}$$

The mode amplitudes should minimize $U_t$, thus

$$\partial(U_t) \geq 0. \tag{28}$$

In order to satisfy (28), the coefficients of the $\partial(A_j)$, $j = 1,5,9,13\ldots$ terms in (27) should be zero, which yields

$$A_1 = -\frac{1}{2} \frac{N_1^2}{N^2 - N_1^2} + \frac{4F}{N_1^2 (N^2 - N_1^2)} \tag{29}$$

$$A_j = \frac{4F}{N_j^2 \left(N^2 - N_j^2\right)}, \quad \mathrm{j} = 5,9,13\ldots. \tag{30}$$

The $\partial(A_j^2)$, $j = 2,3,4,6,7\ldots$ terms in (27) must also satisfy (28), which leads to the following conclusions. First, if its coefficient is positive, $A_j^2$ must be zero to satisfy (28), in which case any variation of $A_j^2$ is positive. Second, if its coefficient is negative, $A_j^2$ must have been constrained to satisfy (28), since any positive variation of $A_j^2$ can invalidate (28). In summary,

$$A_j \begin{cases} = 0, & N^2 < N_j^2 \\ \text{must have been constrained}, & N^2 > N_j^2 \\ \text{can take any value as long as} & N^2 = N_j^2 \end{cases} \quad \mathrm{j} = 2,3,4,6,7\ldots. \tag{31}$$

For practical reasons, only the second mode can be easily constrained mechanically without affecting the first mode, so the second condition of (31) dictates that $j$ can only take the value of 2 when the second mode is not constrained, or 3 when the second mode is constrained. Equation (31) permits three kinds of solution. The first kind is

$$\begin{cases} F = F_1 \\ N^2 < \begin{cases} N_1^2, & \text{with second mode constrained} \\ N_2^2, & \text{with second mode not constrained} \end{cases} \\ A_j = 0, \quad j \neq 1,5,9,13\ldots \end{cases} \tag{32}$$

the second kind is

$$\begin{cases} F = F_2 \\ N^2 = N_2^2 \\ A_j = 0, \quad j \neq 1,2,5,9,13\ldots \end{cases} \tag{33}$$

and the third kind is

$$\begin{cases} F = F_3 \\ N^2 = N_3^2 \\ A_j = 0, \quad j \neq 1,3,5,9,13\ldots \end{cases}. \tag{34}$$

Equations (21), (23), (29), (30), (32), (33) and (34) define the $F-\Delta$ relation of the curved beam. Neglecting the higher modes in (30), closed form solutions can be obtained. Keeping the higher order modes, however, gives a better result. Both solutions are discussed and compared hereafter.

The denominator of (30) is orders of magnitude larger than in (29), so for simplicity, all the higher order terms are temporarily neglected

$$A_j = 0, \quad \mathrm{j} = 5,9,13\ldots. \tag{35}$$

From (21), (29), (32), and (35), the first kind of solution is

$$F_1 = \frac{3\pi^4 Q^2}{2} \Delta \left( \Delta - \frac{3}{2} + \sqrt{\frac{1}{4} - \frac{4}{3Q^2}} \right) \left( \Delta - \frac{3}{2} - \sqrt{\frac{1}{4} - \frac{4}{3Q^2}} \right). \tag{36}$$

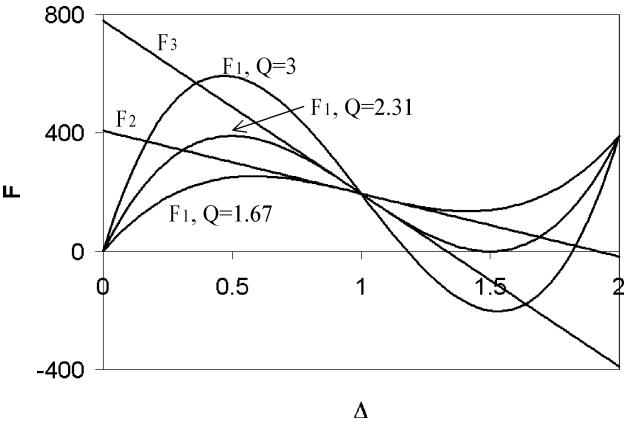


Fig. 3. Several solutions of curved beam normalized force-displacement relation.

From (23), (29), and (32), the normalized axial force with the curved beam at either stable position is

$$(N^2)_{F_1=0}=0, \quad \text{or } N_1^2\left[1+\frac{3Q^2}{8}\left(1-\sqrt{1-\frac{16}{3Q^2}}\right)\right]. \tag{37}$$

From (21), (23), (29), and (33)

$$F_2=\frac{N_1^2\left(N_2^2-N_1^2\right)}{8}\left(\frac{N_2^2}{N_2^2-N_1^2}-\Delta\right)=4.18\pi^4-2.18\pi^4\Delta \tag{38}$$

which exists if both the second mode is not constrained and, by (23), (29), and (33), $Q>2N_2/\sqrt{3}N_1=1.67$. From (21), (23), (29), and (34)

$$F_3=\frac{N_1^2\left(N_3^2-N_1^2\right)}{8}\left(\frac{N_3^2}{N_3^2-N_1^2}-\Delta\right)=8\pi^4-6\pi^4\Delta \tag{39}$$

which exists if both the second mode is constrained and, by (23), (29), and (34), $Q>2N_3/\sqrt{3}N_1=2.31$.

The $F_1$, $F_2$, and $F_3-\Delta$ relations are shown in Fig. 3, all of which are extrapolated to the whole range of $\Delta=0$ to 2. $F_2$ and $F_3$ are straight lines with a negative slope that do not depend on $Q$. $F_3$ can exist only if mode 2 is constrained. $F_1$ depends on Q, but its values at $\Delta=0$, 1, 2 are constants. Moreover, at $\Delta=1$, $F_1$, $F_2$ and $F_3$ pass through the same point. The higher the $Q$, the higher the curving of $F_1$. With $Q=1.67$, $F_1$ becomes tangential to $F_2$ at $\Delta=1$. With $Q=2.31$, $F_1$ becomes tangential to $F_3$ at $\Delta=1$. When $Q$ is larger than those tangential values, curve $F_1$ has two more intersections with either $F_2$ or $F_3$ besides $\Delta=1$. These two additional intersections are where the axial force equals that of the second mode or the third mode. Between these two intersections, either $F_2$ or $F_3$ exists, while outside this interior range of $\Delta$, only $F_1$ exists. The actual $F-\Delta$ curve is therefore a hybrid curve that switches between the $F_1$ curve and either the $F_2$ or $F_3$ curve at these two intersections. The $F_2$ curve is always above zero force except for its small negative value before $\Delta=2$, which means that with the second mode free, even with a very high $Q$, the curved beam can be at most marginally bistable. On the other hand, the $F_3$ curve has a large portion below zero force. With the second mode constrained, the curved beam is bistable with $Q>2.31$. With high $Q$, the $F-\Delta$ curve takes the shape of three straight lines. Dimensionalizing the curves shown in Fig. 3 according to (20), the force-displacement curve of a curved beam with the second mode constrained is as shown in Fig. 4. For $Q\geq 6$, the approximate values in Fig. 4 are

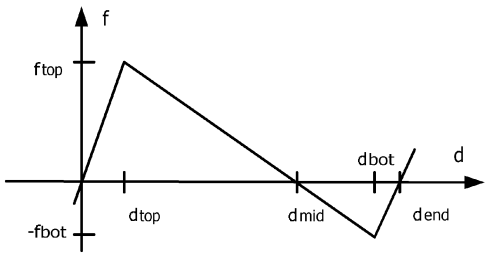


Fig. 4. The f-d curve for a second-mode-constrained curved beam when $Q\gg 1$.

$$f_{\text{top}}\approx 8\pi^4\frac{EIh}{l^3}, \quad f_{\text{bot}}\approx 4\pi^4\frac{EIh}{l^3}, \quad d_{\text{mid}}=1.33h \tag{40}$$

$$d_{\text{top}}\approx\frac{8t}{3Q}, \quad d_{\text{bot}}\approx 2h-\frac{8t}{3Q}, \quad d_{\text{end}}\approx 2h-\frac{4t}{3Q} \tag{41}$$

where (40) is derived from (39), and (41) is derived from (36) and (40). Due to the absence of higher mode terms in (30), both (40) and (41) are only approximate. Moreover, (41) does not give the correct scaling due to this simplification. The next analysis describes the solution with higher modes included, which gives exact expressions for the values shown in Fig. 4.

Keeping all higher order terms in (30), or at least the first two or three terms, would give a more accurate stiffness prediction. From (21), (23), (29), (30), and (32), the first kind of solution should satisfy

$$\sum_{j=1,5,9,13\ldots}\frac{4\left(N^2-N_1^2\right)^2}{N_j^2\left(N^2-N_j^2\right)^2}F_1^2-N_1^2F_1 +\frac{N^2\left(N^2-N_1^2\right)^2}{12Q^2}-\frac{N_1^2N^2\left(N^2-2N_1^2\right)}{16}=0 \tag{42}$$

and (42) can be used to determine $F_1$ from $N^2$. Following this, (21), (29) and (30) can be used to determine the beam shape and hence $\Delta$ from $F_1$. From (21), (23), (29), (30), (33), and (34), both the second kind of solution and the third kind of solution could be obtained, whose forces are still linearly dependent on displacements. Similar curves to those shown in Fig. 3 can be obtained. With high $Q$, the $F-\Delta$ curve again takes the shape of three straight lines. The resulting force-displacement curve of a curved beam with its second mode constrained and with $Q\geq 6$ can still be described by Fig. 4, but with parameters different from those given by (40) and (41). The new parameters are

$$f_{\text{top}}\approx 740\frac{EIh}{l^3}, \quad f_{\text{bot}}\approx 370\frac{EIh}{l^3}, \quad d_{\text{mid}}=\frac{4}{3}h \tag{43}$$

$$d_{\text{top}}\approx 0.16h, \quad d_{\text{bot}}\approx 1.92h, \quad d_{\text{end}}\approx 1.99h \tag{44}$$

Nonlinear finite element analysis (FEA) was performed using Algor. The force-displacement curve from (40) and (41) which neglect the higher modes, the force-displacement curve from (43) and (44) which includes the higher modes, and the FEA results are shown in Fig. 5(a) for a second-mode-constrained curved beam having 3 mm length, 6 $\mu$m thickness, 60 $\mu$m apex

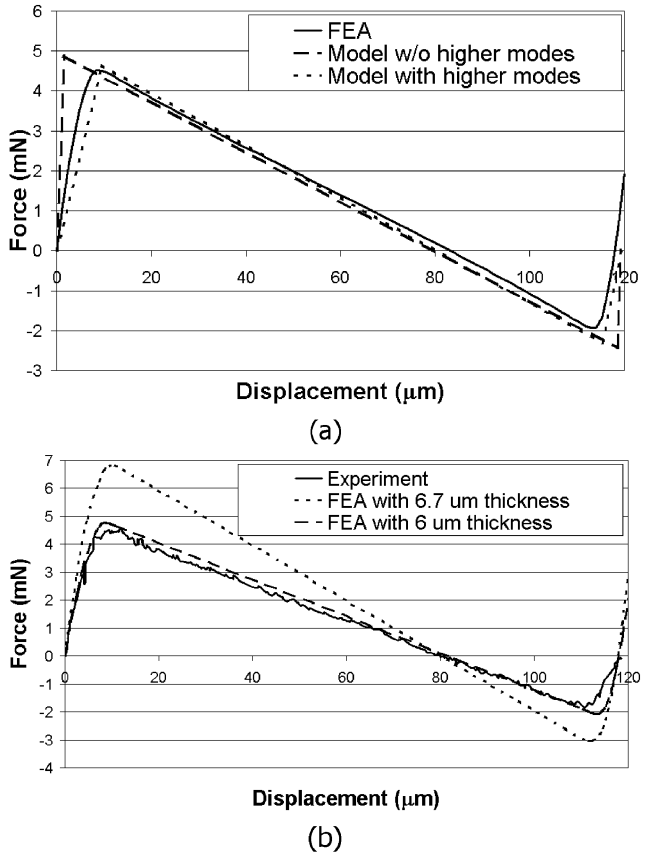


Fig. 5. Comparison of modeled and measured double curved beams f-d curves. (a) Comparison of theoretical models and FEA and (b) comparison of FEA and measurement.

height, 490 $\mu$m depth, and a Young's modulus of 169 Pa. As can be seen, the solution neglecting the higher modes predicts a stiffer curve near both stable positions, while the solution including higher modes agrees very well with FEA.

## III. Design of a Curved-Beam Bistable Mechanism

The structural energy inside the curved beam during deflection comprises both bending energy and compression energy. Qualitatively from an energy viewpoint, the bending energy in the beam increases monotonically whenever the beam is moving downward; while the compression energy increases to a maximum at approximately the centerline, but then decreases after crossing the line. If the beam is designed so that the decrease of compression energy after crossing the centerline is faster than the increase of the bending energy, then a negative force results, which is an indication of bistability.

Based on the last section, a curved beam is bistable if two conditions hold: 1) $Q$ must be large enough and 2) the second mode must be constrained. The first condition is easy to satisfy with DRIE etching since the shape of the beam is only defined by the etching mask. One method to satisfy the second condition is to have a center plunger attached to a single curved beam, and this plunger is guided in an open slot to prevent it from twisting. Another more effective method is to clamp two curved beams together at their centers [6] to provide a double curved-beam structure. The center clamp transfers the rotational motion of either beam center to axial motion of the other beam. Since the beams are stiff in the axial direction, the rotational motion of both beams can be greatly reduced (quenched). The longer the center clamp or the gap between the two beams, the more the second mode can be overcome. With a gap five times larger than the beam thickness, both FEA and microfabricated beams show a visible second mode during the transition, while the f-d curve is still very close to the behavior of a curved beam with the second mode completely constrained. Note that the twisting is only present during the negative stiffness region; at the region close to the two stable positions, the beams move straight even if the center clamp is not long. The bistable double curved beams are shown in Fig. 6(a), while the monostable single beam mechanism is shown in Fig. 6(b). The force-displacement curve of a double curved-beam would just look like what is shown in Fig. 4, with the displacement values equal to, but the force values doubled from, what are given in (43) and (44). Thus,

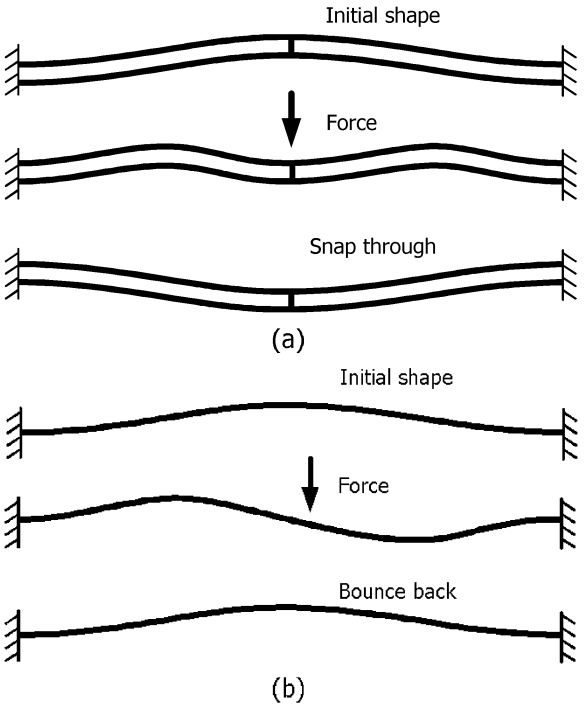


Fig. 6. Bistable double curved beams versus monostable single curved beam. (a) Double curved beams and (b) single curve beam.

$$f_{\mathrm{dbtop}} \approx 1480\frac{EIh}{l^3}, \quad f_{\mathrm{dbbot}} \approx 740\frac{EIh}{l^3}. \tag{45}$$

In designing a curved-beam bistable mechanism to provide a desired force, the maximum strain during deflection should be held within the yield strain of the DRIE etched silicon structure. The maximum strain during deflection can be estimated as

$$\varepsilon_{\max} \approx 2\pi^2\frac{th}{l^2} + 4\pi^2\frac{t^2}{3l^2} = \pi^2\frac{th}{l^2}\left(2 + \frac{4}{3Q}\right) \approx 2\pi^2\frac{th}{l^2}. \tag{46}$$

From (45) and (46)

$$l = \frac{6.31Qf_{dbbot}}{\varepsilon_{\max}^2 Eb} \tag{47}$$

which shows that with a certain force requirement, the length is inversely proportional to the strain squared. A smaller design requires higher fracture strength.

## IV. Optimization of the Curved-Beam Mechanism

The basic double curved-beam design has an asymmetric force-displacement curve, as shown in Fig. 4. In some applications, a more symmetric f-d curve is desired. To examine the asymmetry, define the asymmetry factor r as

$$r = \frac{f_{\text{top}}}{f_{\text{bottom}}}. \tag{48}$$

Then, (40) gives $r = 2$. Note that if we define the asymmetric factor as the ratio of the length of the positive force region and the negative force region, it gives almost the same numerical value. Two approaches have been explored to optimize the double curved-beam mechanism so that $r$ in (48) could be closer to unity. The first approach is to optimize the initial shape of the mechanism. The second approach is to modulate the beam thickness profile along the length of the beams.

Both direct analysis and FEA have been used to try to find an initial shape that includes higher buckling modes that can yield an r closer to unity. However, no improvement has been found. The initial shape involving only the first mode gives the best symmetry. A brief insight into why the inclusion of modes 5, 9, 13... does not help reduce r can be given by examining the role of those modes in the beam behavior. Equation (30) shows that the expressions of $A_{5,9,13...}$ have a large denominator factor $N^2_{5,9,13...} \gg N^2_1$, so $A_{5,9,13...}$ remain neglectable during the beam deflection. But, if there are higher modes with amplitude $\overline{A}_{5,9,13...}$ presented in the initial shape, then instead of (30), the expression for $A_{5,9,13...}$ will be similar to (29) and take the form

$$A_{5,9,13...} = -\overline{A}_{5,9,13...}\frac{N^2_{5,9,13...}}{N^2 - N^2_{5,9,13...}} + \frac{4F}{N^2_{5,9,13...}\left(N^2 - N^2_{5,9,13...}\right)}. \tag{49}$$

With nonzero first term in (49), $A_{5,9,13...}$ would be larger during the beam deflection than it would be in the absence of initial mode amplitude. This enhancement of the mode 5, 9, 13..., according to (23), would lower the increase rate of $N^2$, or compression energy, during the initial beam deflection. The compression energy thus would reach a lower maximum level before decreasing, and its decrease rate afterward would be less significant too. From previous analysis, we know that the faster decrease rate of compression energy than the increase rate of bending energy is the key factor to make the structure bistable. Thus, the bistability is lost or reduced with higher modes included in the initial shape. FEA studies support the conclusion.

Another approach to reduce $r$ involves the modulation of beam thickness. Initial insight into this approach comes again from the model analysis. For the curved beam, the bending energy increases monotonically during the beam deflection, while the compression energy first increases and then decreases during snap-through. It is the dominance of the change of the compression energy over the bending energy that gives bistability. Thus, a beam shape that minimizes the change in bending energy relative to the change in compression energy during beam deflection can help enhance the bistability. The predominant mode in the double-beam deflection is the first mode, which has maximum bending stress near the two boundary clamp sites and the center clamp site. Thus if the thickness at these three locations is decreased, the impact of bending is significantly lowered. Another view of this argument is to consider the three-hinge bistable structure shown in Fig. 7(a). Due to the perfect symmetry of the structure at the up and down positions, the asymmetry factor $r$ is unity. However, it is not easy to implement a perfect hinge with MEMS fabrication, especially when using bulk micro machining. An approximation of the hinged structure is to use thin sections of the beam, which again leads to a design with thin-thick-thin-thick-thin thickness. To avoid dramatic thickness change, a cosine modulation of the thickness is adopted as shown in Fig. 7(b). Thus

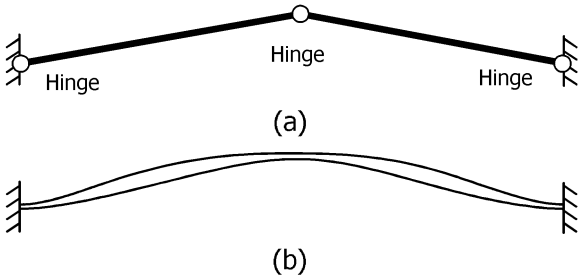


Fig. 7. Concept of curved beam with thickness modulation for better bistability. (a) Three-hinge bistable structure and (b) thickness-modulated curved beam bistable structure.

$$t(x) = t_a\left[1 - \frac{\beta - 1}{\beta + 1}\cos\left(4\pi\frac{x}{l}\right)\right] \tag{50}$$

where $t_a$ is the average thickness of the modulated beam, and $\beta$ is the ratio of the largest thickness and to the smallest thickness. The thin-thick-thin-thick-thin thickness modulation method was discussed and further explored analytically by variation analysis [13].

An FEA study was performed on the thickness modulated single beam. As shown in Fig. 8(a), eight independent curved beams, numbered from top down, with different shapes and constraints are subjected to the center displacement load indicated by arrows. They are all clamped, as indicated by triangles, on both ends. Beams 1, 2, 3, 4 also have their center rotation constrained, as indicated by circles, so their second modes are constrained. All beams have 3 mm length and 60 $\mu$m initial apex height. Beams 4 and 8 have a uniform thickness of 10 $\mu$m. The thicknesses of beams 1, 2, 3, 5, 6, 7 are modulated by a cosine function as in (50) so they all have thin-think-thin-think-thin thickness variations. The average beam thicknesses are still $t_a = 10\ \mu\text{m}$, while the amplitude of the thickness variation is $\beta = 3(t_{\min} = 5\ \mu\text{m}, t_{\max} = 15\ \mu\text{m})$. Though beams 1, 2, 3, 5, 6, 7 have the same thickness profile, they are modulated differently: Beams 3 and 7 only have the bottom edge modulated; Beams 1 and 5 only have the top edge modulated; Beams 2 and 6 have both the top and the bottom edges equally modulated. The FEA force-displacement curves for the mechanisms shown in Fig. 8(a) are shown in Fig. 8(b) for the second-mode-constrained

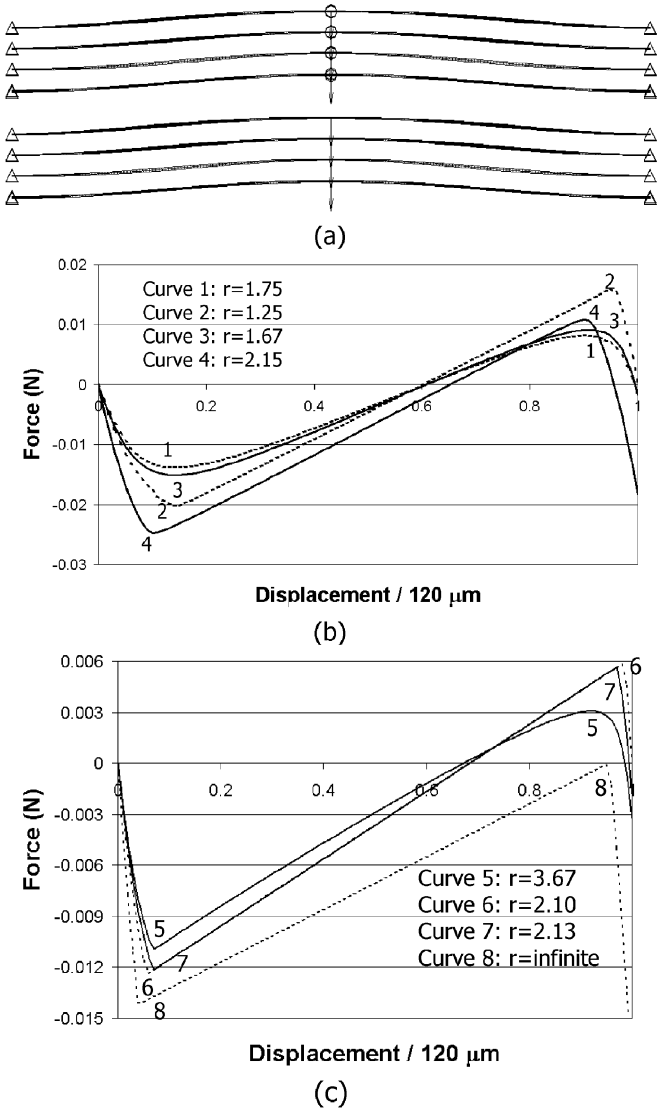


Fig. 8. FEA study for the cosine thickness modulated curved beams. (a) Beam configurations in FEA study, (b) f-d curved of second-mode-constrained beams, and (c) f-d curve of second-mode-free beams.

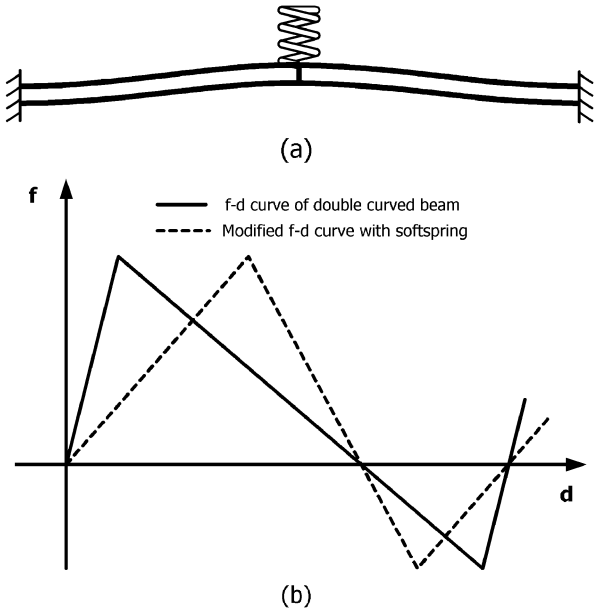


Fig. 9. Double curved beams with softspring. (a) Softspring concept and (b) effect of a linear softspring on the f-d curve of double curved beams.

beams, and in Fig. 8(c) for the second-mode-free beams, where the x-axis is center displacement divided by 120 $\mu$m and the y-axis is force in units of N. It was found that this design does move the asymmetric factor closer to unity. Moreover, it makes the single second-mode-free curved beam bistable. Among the three beam thickness modulations, with both the top and bottom edge modulated, the best optimization result is shown by curves 2 and 6 in Fig. 8. The FEA study also shows that such modulated beams have more stress than the basic double curved beams, with the maximum stress occurring at the thin beam sections. The maximum stress is usually two or three times higher than in a uniform-thickness double curved beams. With $\beta = 3$, the center-constrained curved beam has $r = 1.25$, and the center-free curved beam has $r = 2.1$. To lower the value of $r$, higher values of $\beta$ can be used.

The curved-beam bistable mechanism has an f-d curve in which the maximum force occurs very close to the initial position, and then decreases. This property is not good for some actuators especially electrostatic actuators, whose actuation force starts low and then increases, as the two electrodes get closer. A bistable f-d curve with a gentler ramping up of force may be needed for other reasons too. One way to modify this is to include a soft spring with the curved beam structure as shown in Fig. 9(a). A cantilever attached to the double beam center can realize such a softspring. The spring can be linear or nonlinear, and correspondingly, the f-d curve could be modified in various ways. It should be noted that such softspring does not change the maximum actuation force and the maximum stroke required to snap the bistable structure. Fig. 9(b) shows f-d relations of double curved beams before and after being coupled with a linear softspring. It could be seen that for the actuator to overcome to snap the bistable structure, the energy barrier calculated as the area under the positive force segment will be the same with or without the softspring structure.

## V. Fabrication and Testing

Microscale double curved beams designed by the previous section have been fabricated and successfully tested. The beams described below were designed with a span of $l = 3$ mm, a thickness of $t = 10$ $\mu$m, a depth of $b = 490$ $\mu$m and an initial apex height of $h = 60$ $\mu$m. The estimated maximum strain within the mechanism during snap through is 0.16%.

The experimental mechanism was etched from a (100), double side polished silicon wafer. The orientation of the bistable beams was parallel to the primary flat. In this direction the beams had a Young's modulus of 168.9 Gpa [14]. Fillets were added in the etch mask at the sharp corners to lower the stress concentration. Further, halos were included in the mask, so that the etch space had the same 20-$\mu$m-width throughout the mask. This arrangement helped to ensure that etching occurred at the same rate at all locations. The etch mask itself comprised a 0.75-$\mu$m-oxide hard mask, and a 15-$\mu$m-photo resist soft mask. The etch recipe "MIT69A" was used as developed in the Microsystems Technology Laboratories of MIT. The total time

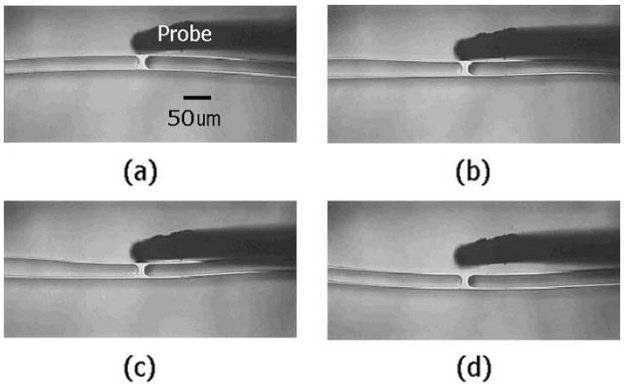


Fig. 10. The bistable mechanism as pushed manually by probe. (a) Double curved beams at its initial stable position, (b) double curved beams deflect, (c) double curved beams deflect more, and (d) beams at second stable position after snap-through.

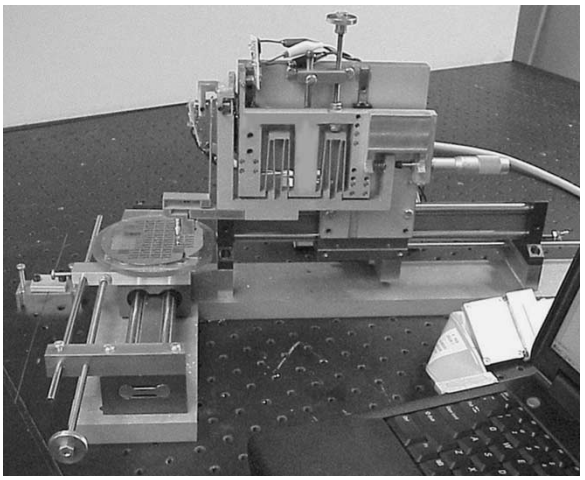

Fig. 11. The specialized MEMS force-displacement tester.

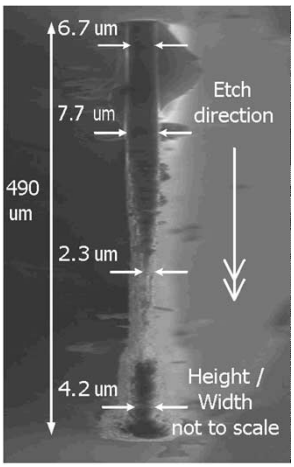


Fig. 12. SEM cross section of a curved beam fabricated with DRIE.

taken to etch through the entire wafer thickness of 490 $\mu$m was about 4.5 h. To help smooth out the sidewall surface roughness created during DRIE, a dry isotropic etch using SF6 for 15 seconds followed the through-etch.

The characteristic parameters of the bistability curves were determined only by the etched beam geometry and the Young's modulus of the wafer. Therefore they could be significantly affected by fabrication variations especially by variation of the beam thickness. The actual beam thickness after fabrication was significantly less than the designed 10 $\mu$m, as shown in the scanning electron microscope (SEM) picture in Fig. 12. As can be seen in the figure, the cross-sectional thickness varied between 2.3 and 7.7 $\mu$m. Note also the eroded structure at the bottom of the beam. The reduction of the fabricated beam thickness from its designed value resulted mainly from the loss of mask coverage during the etch process. Due to the long time for the through-etch, a relatively thick mask resist layer was required. Such a thick resist layer showed slanted sidewalls after exposure and development. During DRIE, the resist was continuously etched away not only from the top surface but also from the sidewalls, which exposed regions on the wafer that are supposed to be protected, hence the reduction in beam thickness. The thickness variation along the wafer depth was consistent with the fact that the DRIE process produces nonideally etched sidewalls. Careful tuning of the etch parameters can result in almost straight sidewalls for a particular process, but after days or weeks during which the condition of the etch changes, the etched sidewall became nonideal again even with the same recipe.

A micro probe was used to push the experimental mechanism down and up at its center. The two stable positions of the mechanism, together with two middle positions while being pushed down are shown in Fig. 10; only the center portion of the mechanism is shown. Several single curved beams, and several double curved beams with low Q value, were also fabricated on the wafer, but probing of such structures showed that none of them are bistable.

To measure the force-deflection characteristics of the experimental bistable mechanisms, a specialized MEMS force-displacement tester [15], as shown in Fig. 11 was developed. The method used is based on physical contact between the MEMS mechanism and a needle probe. The force and displacement of the MEMS mechanism are detected by the deflection and movement of a calibrated reference flexure holding the needle probe. The parasitic compliance of the needle probe does not affect the measurement accuracy of the force and displacement due to a specialized calibration procedure. The tester featured a resolution of 10 nm for displacement, and 100 $\mu$N for force. A total of 20 force-displacement measurements were performed on ten bistable mechanisms with the same design geometry at different locations on the same wafer. For each measurement, the bistable mechanism was pushed from both sides, since at the snap through point, it moves away from the probe tip. The overall force-displacement curve was found by "stitching" the two measurement sets together.

The behavior of the bistable mechanism was measured and predicted by two-dimensional (2-D) FEA, as shown in Fig. 5(b). The solid curve is one of the measurement results, while the dotted and dashed curves are FEA results for beam thickness of 6.7 $\mu$m and 6 $\mu$m, which are the top thickness and average cubic thickness of the fabricated beam shown in Fig. 12, respectively. Cubic average thickness gives good prediction of the stiffness of a nonuniform cross-section beam, because the beam stiffness is proportional to the moment of inertia $I$, which has a cubic

dependence on beam thickness. Note that the top thickness of the beam could be measured by a microscope with a scale, but a detailed knowledge of the beam thickness variation along the depth could only be obtained destructively. It can be seen that the measured curve suggests less force than the FEA prediction for 6.7 $\mu$m thick beams, but it is very close to the prediction for 6 $\mu$m thick beams.

The fabrication and testing of curved beam mechanisms proves the validity of the theoretical analysis. It also shows that to design an accurate force-displacement characteristics of the bistable structure, fabrication variance must be taken into account. It is difficult to model a curved beam with varying thickness, such as shown in Fig. 12, by either theoretical analysis or finite element analysis, but as the measurement shows, a cubic average thickness gives a very good approximation for the f–d characteristics of such structures.

## VI. Summary and Conclusion

This paper has proposed, analyzed, designed and fabricated a bistable mechanism that does not rely on hinges, latches or as-fabricated internal stress for its bistability. The mechanism comprises only a pair of initially cosine-shaped parallel beams that are clamped together at their centers. Such a mechanism appears to be well suited for use in applications such as relays, valves, clips etc. Further, it should be possible to extend the mechanism to two dimensions in the form of initially curved but parallel plates.

A buckling-beam based analysis of the mechanism was used to support its design. This analysis resulted in a relation between the force applied to, and the deflection of, the center of the mechanism. It is interesting to note that the character of this relation is dependent only on the single parameter Q when the beam deflections are properly normalized. Further, beam thickness modulation and softspring coupling were introduced as means of making the force-displacement characteristic of the mechanism more desirable. The analytical methods developed for the design of bistable double beams were shown to be accurate and to provide insight into the behavior of such systems. It was the analysis of a single beam without prestress that revealed the unstable second mode, which inspired the design synthesis process of using one beam's unstable mode to quench that of another. Such insight is not gained by FEA, which is a valuable confirmation and optimization tool; hence illustrating that continuum mechanics plays a strong and vital role in the development of MEMS mechanisms.

Finally, experimental microscale mechanisms were fabricated from single-crystal silicon wafers using deep-reactive ion etching. The mechanisms exhibited the expected bistability. Further, the details of their force-deflection relations were well matched to those predicted by the buckling beam analysis, which were in turn both well matched to those predicted by FEA. This demonstrates the validity of the analysis and the general observations made above.

## Acknowledgment

This work is based on Dr. J. Qiu's Ph.D. dissertation [16].

## References

[1] M. Hoffmann, P. Kopka, and E. Voges, "All-silicon bistable micromechanical fiber switch based on advanced bulk micromachining," *IEEE J. Select. Topics Quantum Electron.*, vol. 5, no. 1, pp. 46–51, 1999.

[2] X. Sun, K. Farmer, and W. Carr, "A bistable microrelay based on two-segment multimorph cantilever actuators," in *Proc. IEEE MEMS 1998 Conference*, pp. 154–159.

[3] B. Jensen, M. Parkinson, K. Kurabayashi, L. Howell, and M. Baker, "Design optimization of a fully-compliant bistable micro-mechanism," in *Proc. 2001 ASME International Mechanical Engineering Congress and Exposition 1–7*.

[4] E. Kruglick and K. Pister, "Bistable MEMS relays and contact characterization," in *Proc. Solid-state Sensors and Actuators Workshop*, Cleveland, OH, 1998, pp. 333–337.

[5] M. Taher, "On a tunable bistable MEMS-theory and experiment," *Journal of MEMS*, vol. 9, no. 2, pp. 157–170, 2000.

[6] M. Vangbo, "Analytical analysis of a compressed bistable buckled beam," *Sens. Actuators, Phys. A*, vol. 69, no. 3, pp. 212–216, 1998.

[7] Y. Yang and C. J. Kim, "Testing and characterization of a bistable snapping microactuator based on thermo-mechanical analysis," *Proc. Solid-State Sensors Actuators*, pp. 337–340, 1995.

[8] B. Wagner, H. Quenzer, S. Hoerschelmann, T. Lisec, and M. Juerss, "Bistable microvalve with pneumatically coupled membranes," in *Proc. IEEE MEMS 1996 Conference*, pp. 384–388.

[9] J. Qiu, J. Lang, and A. Slocum, "A centrally-clamped parallel-beam bistable MEMS mechanism," in *Proc. IEEE MEMS 2001 Conference*, pp. 353–356.

[10] J. Qiu, J. Lang, A. Slocum, and R. Struempler, "A high-current electrothermal bistable MEMS relay," in *Proc. IEEE MEMS 2003 Conference*, pp. 64–67.

[11] J. Lee, M. Lee, W. Jang, C. Choi, and J. Joo, "Bi-stable planar polysilicon microactuators with shallow arch-shaped leaf springs," in *Proc. SPIE Conference on Micromachined Devices and Components V*, 1999, pp. 274–279.

[12] L. Dellmann, W. Noell, C. Marxer, K. Weible, M. Hofmann, and N. Rooij, "4 × 4 matrix switch based on MEMS switches and integrated waveguides," *Proc. Solid-State Sensors Actuators*, pp. 1332–1335, 2001.

[13] M. Brenner, J. Lang, J. Li, J. Qiu, and A. Slocum, "Optimum design of a MEMS switch," in *Proc. 5th International Conf. on Modeling and Simulation of Microsystems*, USA, April 2002.

[14] J. Kim, D. Cho, and R. Muller, "Why is (111) silicon a better mechanical material for MEMS," in *Proc. Transducers 2001*, pp. 662–665.

[15] J. Qiu, J. Sihler, J. Li, M. Smith, V. Sturgeon, and A. Slocum, "An instrument to measure the stiffness of MEMS mechanisms," in *Proc. 10th International Conference on Precision Engineering*, Yokohama, Japan, July 2001, pp. 599–603.

[16] J. Qiu, "A Thermally-Actuated Bistable MEMS Relay for Power Applications," Ph.D. dissertation, Dept. Mechanical Eng., Massachusetts Inst. Technol., Cambridge, June 2003.

**Jin Qiu** received the Ph.D. degree in mechanical engineering from Massachusetts Institute of Technology (MIT), Cambridge, in 2003, with a minor in business. He also received the B.S. degree in electrical engineering from Nanjing University in 1997 and the M.S. degree in mechanical engineering from MIT in 1999.

He studied and worked in several MIT labs including Precision Engineering Research Group, Microsystems Technology Laboratories, Laboratory for Electromagnetic and Electronic Systems, and Acoustics and Vibrations Laboratory. His interests focus on the development of MEMS, compliant structures, and power electronics. His doctoral project resulted in two pending patents, and was ranked top one among 20 others by its industry sponsor, a global power and automation company. He joined Tyco Electronics, Menlo Park, CA, in 2003.

**Jeffrey H. Lang** (S'78–M'79–SM'95–'F'98) received the S.B., S.M., and Ph.D. degrees in electrical engineering from the Massachusetts Institute of Technology (MIT), Cambridge, in 1975, 1977, and 1980, respectively.

Currently, he is a Professor of Electrical Engineering at MIT. He has been an MIT faculty member since receiving his Ph.D. degree and his research and teaching interests focus on the analysis, design, and control of electromechanical systems with an emphasis on rotating machinery, microsensors and actuators, and flexible structures. He has written over 160 papers and holds 10 patents in the areas of electromechanics, power electronics, and applied control.

Dr. Lang and has been awarded four Best Paper prizes from various IEEE societies. He is a former Hertz Foundation Fellow and a former Associate Editor of *Sensors and Actuators*.

**Alexander H. Slocum** (M'03) received the Ph.D. degree from the Massachusetts Institute of Technology (MIT), Cambridge, while simultaneously working from 1983 to 1985 at the National Bureau of Standards, where he also earned 12 superior service awards and a Department of Commerce Medal.

He is currently a Professor of Mechanical Engineering at MIT and a MacVicar Faculty Fellow. He has about 60 patents issued/pending and he designs manufacturing equipment for the automotive, aerospace, semiconductor, and entertainment industries. He has been involved in several manufacturing equipment company start-ups, and he has helped many different companies bring many different machines to the marketplace. In addition, he has also been involved with nine products that have been awarded R&D 100 awards, each for annually being one of one hundred most technologically significant new products. His research has involved three dozens Ph.D. students. His current interests focus on the development of instruments, MEMS, and nanotechnology.

Dr. Slocum is the recipient of the Society of Manufacturing Engineer's Frederick W. Taylor Research Medal.